Available online at www.sciencedirect.com
SCIENCE DIRECT
Journal of Catalysis 232 (2005) 247–256
JOURNAL OF CATALYSIS
www.elsevier.com/locate/jcat

$Sr_{1-x}Ag_xTiO_{3\pm\delta}$ ($x = 0$, 0.1) perovskite-structured catalysts for the flameless combustion of methane

L. Fabbrini [a], A. Kryukov [b], S. Cappelli [a], G.L. Chiarello [a], I. Rossetti [a], C. Oliva [a], L. Forni [a,*]

[a] *Dipartimento di Chimica Fisica ed Elettrochimica, Università di Milano via C. Golgi, 19 I-20133 Milano, Italy*
[b] *D.I. Mendeleev University of Chemical Technology of Russia, Moscow, Russia*

Received 25 January 2005; revised 4 March 2005; accepted 14 March 2005

Available online 22 April 2005

Abstract

Several samples of $Sr_{1-x}Ag_xTiO_{3\pm\delta}$ ($x = 0$, 0.1) perovskite-structured catalysts were prepared and tested for the title reaction under lean-burn conditions. For the same overall nominal composition, catalyst activity and durability depend strongly on the method of preparation and, for the samples prepared by the same method, mainly on temperature and on the residence time at such a temperature during preparation. In $Sr_{0.9}Ag_{0.1}TiO_{3\pm\delta}$ catalysts Ag is present either as intra-crystalline Ag^{2+}, likely substituting for Sr^{2+} in the perovskite lattice, or as inter-crystalline metallic Ag. The catalytic activity of $Sr_{0.9}Ag_{0.1}TiO_{3\pm\delta}$ is connected with the presence of O_2^-/Ti^{4+}, O_x^-/Ag, and O_x^-/Ag^{2+}; of O_3^-/Ti^{4+}, O^-/Sr^{2+}; or of O^-/Ti^{4+} species, depending on preparation method and conditions. Furthermore, inter-crystalline metallic Ag plays an important role in improving catalyst resistance to sintering; the most durable samples are those calcined for a sufficient residence time at the highest temperature during preparation, that is, under conditions more favourable to the segregation of this metal from the perovskite lattice.

Keywords: Perovskite-structured mixed oxides; Sr-titanate and Ag-doped Sr-titanate; Catalytic flameless combustion of methane

1. Introduction

The catalytic flameless combustion (CFC) of hydrocarbons represents the most efficient way to exploit the chemical energy of hydrocarbons by oxidation of fuel/air lean mixtures, while substantially reducing or even virtually suppressing any formation of NO_x [1–3]. Indeed, at low temperatures nitrogen oxides are thermodynamically unstable and hence they cannot form during combustion. Thus, provided the combustion is carried out at a sufficiently low temperature (< 800 °C), any need for post-combustion NO_x abatement is eliminated. The efficiency of noble metals, especially of Pt, as catalysts for the CFC of hydrocarbons has been well known since the pioneering work of Faraday and Davy [4], and these metals are still extensively studied [5] for the present reaction, because of the increasingly severe restrictions imposed to improve the quality of air. However, the booming price of noble metals, due to the enormously growing demand during the last three decades, has stimulated an intensive search for low-cost substitutes for these catalysts. Among the various potential substitutes, some classes of transition-metal oxide mixtures, especially with perovskite-like structures, appear very promising [6,7].

Since the late 1990s our research group has prepared and tested several kinds of mixed oxides, with the CFC of methane as a test reaction, focusing particularly on $A_{1-x}A'_xBO_3$ (A = La, Sr; A′ = Ce, Eu, Sr; B = Co, Mn, Fe, Ni) perovskite-structured oxides [8–17]. During this work, in addition to the traditional calcination-milling [18] and sol–gel-citrates (SGC) [19] methods, we have proposed an innovative flame hydrolysis (FH) preparation procedure [11], and, more recently, the flame-spray pyrolysis (FP) method [20,21] has been applied. Furthermore, an extensive study has been carried out in our laboratory on the anchoring

* Corresponding author. Fax: +39 02 50314300.
E-mail address: lucio.forni@unimi.it (L. Forni).

0021-9517/$ – see front matter
doi:10.1016/j.jcat.2005.03.012

of the same catalysts on a cordierite honeycomb monolith support, through a proper primer, that is, on preparing the catalyst in the form usually selected for practical application [16,17].

Among the most recently tested catalysts, $SrTiO_3$ was shown to be very active for the CFC of methane [22], and its activity was found to further improve when Ag was partially substituted for Sr. This prompted us to undertake the present deeper investigation of these Sr-titanate and Ag–Sr-titanate catalysts, with the goal of correlating their performance with their physical–chemical characteristics. Furthermore, since the durability of any catalyst for the present reaction represents a particularly important feature for practical application, special attention was also paid to catalyst resistance to decay.

2. Experimental

2.1. Catalyst preparation

A first set of catalysts was prepared by the SGC technique. However, a particular procedure [23] was needed for the present materials, because of the sensitivity of Ti^{4+} ion to water, causing the immediate precipitation of TiO_2. Briefly, 5 cm^3 of Ti-iso-propoxide (Fluka; purum) was dropped very slowly into 50 cm^3 of vigorously stirred distilled water. To the so obtained suspension of freshly precipitated $TiO_2 \cdot H_2O$, 3 mol of citric acid (Fluka; 99.5% pure) was added per 2 mol of Ti ions, followed by a few cm^3 of hydrogen peroxide (Aldrich; 30 vol% aqueous solution), until the precipitate dissolved completely. A stoichiometric amount of Sr^{2+} ions was then added, from a solution we prepared by dissolving $Sr(CH_3COO)_2$ (Acros; > 99% pure) in a minimum of distilled water and adding citric acid to obtain an acid/Sr molar ratio of 1:3. The complexation of metallic ions by citric acid prevented any re-precipitation of TiO_2. The perfectly clear final solution was evaporated in vacuo (residual pressure 70 Torr; 1 Torr = 133 Pa) at 35–40 °C in a rotavapor, until a gel was formed and then at 70 °C until a yellow powder was formed. The latter was divided into two portions and calcined in flowing air (50 cm^3/min) under different conditions. The first batch was calcined as the temperature was increased by 0.5 °C/min from 25 to 250 °C, maintained for 1 min, then increased by 1 °C/min to 950 °C, and then maintained for 60 min. The second batch was calcined as the temperature was increased by 0.5 °C/min from 25 to 250 °C, maintained for 1 min, then increased by 3 °C/min to 850 °C, and then maintained for 60 min. The two catalysts so obtained are referred to as SGC-1 and SGC-3 (Table 1), respectively.

We prepared a second set of catalysts by slowly dropping the Ti-iso-propoxide directly into a vigorously stirred aqueous solution of citric acid (acid/Ti molar ratio = 2:1). The fresh $TiO_2 \cdot H_2O$ precipitate rapidly dissolved with the addition of a few cm^3 of the previously mentioned hydrogen peroxide solution. To the clear, orange-coloured solution so obtained, a solution of Ag-nitrate and Sr-acetate was added, which we prepared by dissolving $AgNO_3$ (Carlo Erba; 99.8% pure) and $Sr(CH_3COO)_2$ in a minimum of water and then adding citric acid in a 2:1 molar ratio, with respect to the sum of Ag^+ and Sr^{2+} ions. The perfectly clear final solution was evaporated in a rotavapor as previously described, and the powder obtained was divided into three portions, which were calcined as follows in air flowing at 50 cm^3/min: after a first step in which the temperature was increased by 0.5 °C/min from 25 to 250 °C and maintained for 1 min for each sample, the temperature was increased to 850 °C and then maintained for 60 min. The rates of temperature increase for the second heating step were 1, 2.5, and 5 °C/min, respectively, for the three batches. These three catalysts are referred to as AgSGC-1, AgSGC-2.5, and AgSGC-5, respectively (Table 1).

A further sample, designated AgFH (Table 1), was prepared by the FH technique. This has been described in detail elsewhere [11]. Briefly, a diluted (3 wt%) aqueous solution, prepared as described (vide supra) and containing citric acid and the Sr, Ti, and Ag ions in the desired ratios, was nebulised in a H_2–O_2 flame. At the high temperature ($\geqslant$ 1600 °C) of the flame the solvent vaporises instantaneously and the perovskite–structured oxide mixture forms spheroidal nanoparticles, collected by means of an electrostatic precipitator.

A final couple of catalysts (FP and AgFP, respectively; Table 1) were prepared by the FP method. The procedure has been extensively described elsewhere [20,21]. Briefly, solutions of $Sr(NO_3)_2$, dissolved in propionic acid; of Ti-isopropoxide, dissolved in 2-ethyl-hexanoic acid; and, when required, of $AgNO_3$, dissolved in acetonitrile, were combined in the desired ratios to obtain an overall concentration of the metallic ions of 0.05 M. The combined solution was then fed by means of a syringe pump (Harvard 975) to a capillary tube (1 mm OD, 0.6 mm ID), ending in the centre of a vertical nozzle (1.1 mm in diameter), to which a constant flow of oxygen (SIAD; purity grade 4.0) was fed. The flame was started and kept stable by a ring of premixed O_2–CH_4 flamelets surrounding the main nozzle. The organic solution sprayed within the oxygen jet of the nozzle instantaneously

Table 1
Some relevant characteristics of the catalysts prepared and tested. $T_{1/2}$ = temperature of 50% CH_4 conversion during standard activity tests

Catalyst	Nominal composition	S_{BET} (m^2/g)	Agglomerated nanoparticle clusters size (nm)	$T_{1/2}$ (°C)
SGC-1	$SrTiO_3$	1	30–400	573
SGC-3	$SrTiO_3$	28	30–200	525
AgSGC-1	$Sr_{0.9}Ag_{0.1}TiO_3$	21	30–100	441
AgSGC-2.5	$Sr_{0.9}Ag_{0.1}TiO_3$	22	30–100	430
AgSGC-5	$Sr_{0.9}Ag_{0.1}TiO_3$	24	30–100	400
AgFH	$Sr_{0.9}Ag_{0.1}TiO_3$	12	50–800	542
FP	$SrTiO_3$	107	30–60	520
AgFP	$Sr_{0.9}Ag_{0.1}TiO_3$	67	30–60	402

vaporises and ignites, ending in a spheroidal nanoparticle powder of the oxide mixture, collected by means of the previously mentioned electrostatic precipitator.

Some relevant characteristics of the catalysts that were prepared and investigated are collected in Table 1.

2.2. Catalyst characterisation

The solid phases were recognised and their degree of purity determined by X-ray diffraction (XRD) analysis, by means of a Philips PW1820 powder diffractometer, operated at 40 kV and 40 mA, with Ni-filtered, Cu-K_α radiation ($\lambda = 1.5418$ Å). The oxide particle size and shape were determined by scanning electron microscopy (SEM), with a Cambridge Stereoscan 150 or a Leica LEO 1430 instrument. The specific BET surface area (S_{BET}) was measured by nitrogen adsorption-desorption at liquid nitrogen temperature, with a Micromeritics ASAP 2010 instrument. Electron paramagnetic resonance (EPR) spectra were collected with a Bruker Elexsys instrument, equipped with a standard rectangular ER4102ST cavity and operated at 9.4 GHz, 1 mW microwave power, and 1 Gauss modulating amplitude and in the temperature range of −173 and 25 °C. The intensity of the magnetic field was carefully checked with a Bruker ER35M teslameter, and the microwave frequency was measured with a HP 5340A frequency meter.

2.3. Catalytic activity and thermal stability tests

Catalytic activity comparison tests have been carried out under rigorously standard experimental conditions (vide infra) with a bench scale apparatus, centred on a continuous, tubular, down-flow quartz reactor (0.7 cm ID, 40 cm long). For every run we diluted in 1.3 g of 60–100-mesh quartz powder 0.2 g of catalyst, which we prepared by pressing (3 tons/cm^2) the original nanoparticle powder into wafers, which were then crushed and sieved to 60–100-mesh particles. The catalyst bed was kept in the middle, isothermal portion of the reactor tube by small flocks of quartz wool, and the void space above and below the catalyst bed was filled with 10–20-mesh quartz beads. The reactor was heated by an electric furnace, controlled with a Eurotherm 812 TRC, governed by a thermocouple fitted within the heavy metal blocks surrounding the reactor tube. Before the reaction the catalyst was activated in situ in air flowing at 20 cm^3/min, as the temperature was increased by 10 °C/min to 650 °C and maintained for 1 h. After temperature was lowered to 250 °C, the gas flow was switched to a 20 cm^3/min gas mixture composed of 10 cm^3/min of 1.04 vol% CH_4 in He (SIAD; certified mixture) and 10 cm^3/min of air (SIAD; purity grade 5.0), and the test run was immediately started as the temperature was increased by 2.3 °C/min to the temperature (T_f) of CH_4 full conversion. The selected value of the time factor $\tau = W/F$, where W is the catalyst weight (g) and F (cm^3/min) is the overall gas flow rate, was 0.6 $g_{cat}\,s/cm^3_{flowing\ gas}$ for every test run. During any of the runs conversion of CH_4 was monitored every 10 min through gas chromatographic analysis of the outlet gas, carried out by means of an on-line HP 5890 instrument, equipped with a thermal conductivity detector and with two columns (1/8″ OD, 2 m long) in series, packed with Porapak Q and MS-5A, respectively.

The thermal stability accelerated tests were carried out at the end of the standard test runs, during which the temperature was kept at T_f and methane conversion was checked after 100 h on stream. Then the catalyst was subjected to several overheating/reaction cycles, in which the temperature was increased by 10 °C/min to 800 °C, kept for 1 h, and then lowered to T_f for at least 0.5 h before the methane conversion was checked again. Neither oxidation products different from CO_2 nor traces of nitrogen oxides of any composition were ever detected in the outgoing gas, for any of the activity comparison or thermal stability test runs.

3. Results and discussion

3.1. Catalyst characterisation

The S_{BET} of the various catalysts is given in Table 1. It may be noticed that the value of this parameter depends strongly on the method of preparation and, for the samples prepared by the same method, on composition and mainly on residence time and temperature attained during preparation. The higher the latter two parameters were, the more sintered the sample became. Indeed, SGC-1, which was calcined for 2 h at 950 °C, showed a very small value (1 m^2/g) of S_{BET}, whereas for SGC-3, AgSGC-1, AgSGC-2.5, and AgSGC-5, which were calcined for 1 h at a temperature 100 °C lower only, values of S_{BET} ranging from 21 to 28 m^2/g were obtained. For the AgFH sample, prepared at very high flame temperature (⩾1600 °C), but with a very short residence time (on the order of 1 ms), S_{BET} was 12 m^2/g. On the other hand, values of S_{BET} up to one order of magnitude higher were obtained with the samples prepared by the FP technique, that is, with a similarly short residence time, but with a lower flame temperature (≅1400 °C), because of the lower heat of combustion of the organic solvents employed, with respect to pure hydrogen. Furthermore, among the Ag-doped SGC samples, a small increase in S_{BET} can be noticed for a more rapid rate of temperature increase during calcination, which is likely due to an increasing structural disorder of the solid, conferred by the progressively increasing heating rate.

The XRD patterns of the various catalysts are collected in Fig. 1. All of them were shown to possess the perovskite-like structure [24]. For the Ag-doped samples this was accompanied by stronger or weaker peaks at $2\theta = 38.2°, 44.5°, 64.5°$, characteristic of the metallic Ag fcc phase [25]. Indeed, all of the Ag-doped samples, regardless of the preparation procedure, showed a stronger or fainter vi-

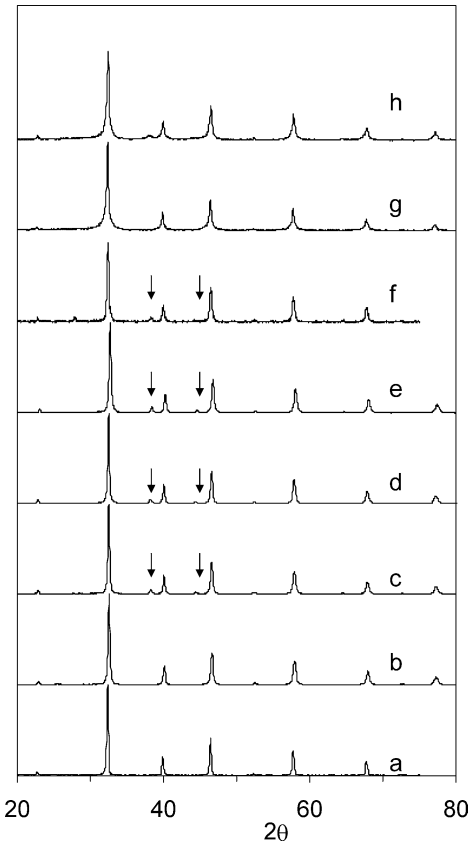

Fig. 1. XRD patterns of the various catalysts. (a) to (h): SGC-1, SGC-3, AgSGC-1, AgSGC-2.5, AgSGC-5, AgFH, FP, AgFP, in the order. All the patterns have been normalised as I/I_0. I_0 values (counts): (a) 1800, (b) 6280, (c) 6590, (d) 6000, (e) 6100, (f) 600, (g) 2850, (h) 2750. Arrows indicate the main reflections of metallic Ag fcc phase.

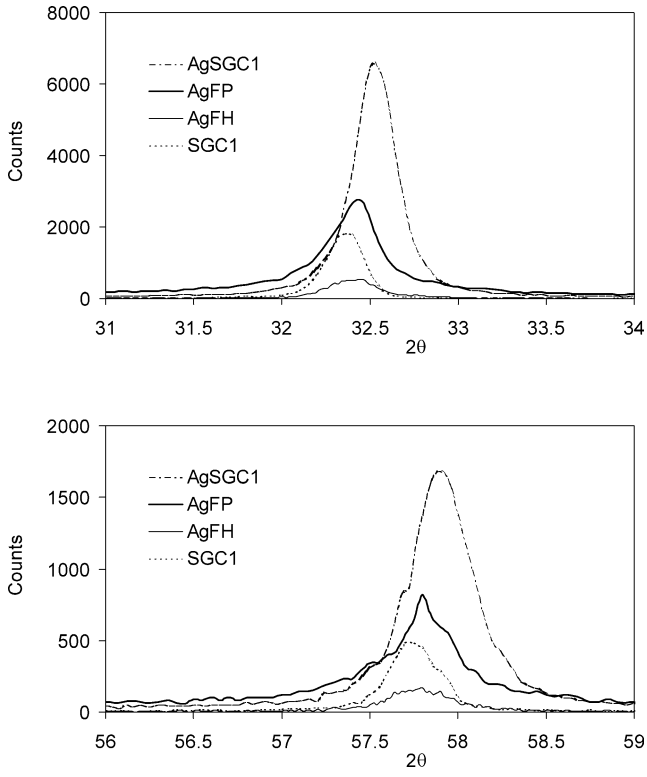

Fig. 2. Comparison between the enlarged XRD patterns of SGC-1, AgFH, AgFP and AgSGC-1 catalysts. Upper part: main reflection (I_0); lower part: reflection at 2θ around 50°.

olet hue, characteristic of the basically white Ag-containing compounds, in which Ag ions partially reduce to metal, which then segregates from the main phase. Furthermore, when we compared the enlarged XRD patterns of the Ag-doped samples, prepared on one hand by the FH and FP procedures and, on the other hand, by the SGC technique, a difference in 2θ up to 0.25° was noticed for the same reflection (see, e.g., Fig. 2, upper part), with respect to the undoped catalyst. The shifting is perfectly confirmed by the main reflection at $2\theta > 50°$ (Fig. 2, lower part). This indicates that Sr^{2+} (ionic radius 1.13 Å) has been partially replaced by Ag^{2+} (ionic radius 1.08 Å), so that the cell volume became smaller, causing the shift of the XRD reflection peaks to higher 2θ values, in line with the so-called Vegard generalisation. In addition, Fig. 2 shows also that a much lower degree of Ag^{2+} substitution for Sr^{2+} in the perovskite lattice has occurred for the AgFH and AgFP samples, with respect to the AgSGC samples. Indeed, a calculation relative to the latter samples showed that most of the Ag (e.g., up to 60% of the nominal amount for the AgSGC-1 sample) was present as intracrystalline framework Ag^{2+} in the perovskitic lattice. This is very likely a consequence of the less severe SGC preparation conditions for the solid, with respect to either the FH or the FP method, allowing the perovskitic lattice of the AgSGC sample to allocate a higher amount of extraneous ions. As a vicar of the Sr^{2+} ion, the lattice Ag^{2+} ion is forced to assume this unusual charge by the perovskite crystal field force. Because of the difference in ionic radii (vide supra), however, the perovskitic structure permits the accommodation of such ions within a rather low substitution degree only, depending on the method of preparation. Because of the high-temperature instability of Ag oxides and the relatively low melting point of metallic silver, it cannot be excluded that part of the silver was lost during high-temperature synthesis (FH and FP techniques). In the worst case (FH sample) the percentage of this lost Ag, determined by chemical analysis, was ca. 50 wt% with respect to the nominal amount. Furthermore, some Ag was segregated in metallic extraframework form, as indicated by XRD analysis.

SEM micrographs (Fig. 3) showed that all of the catalysts were composed of spheroidal nanoparticles, more or less clustered into larger agglomerates. The size of the latter was larger for the samples prepared by the SGC method (up to 400 nm) and especially by the FH technique (up to 800 nm), and smaller (30–60 nm) for those prepared through the FP method. This is roughly in line with the different values of S_{BET} of the various catalysts (Table 1). The higher the average particle size was, the lower was the S_{BET} value; this means that the total specific surface area was essentially due to the external surface of the nanoparticles, which were substantially nonporous.

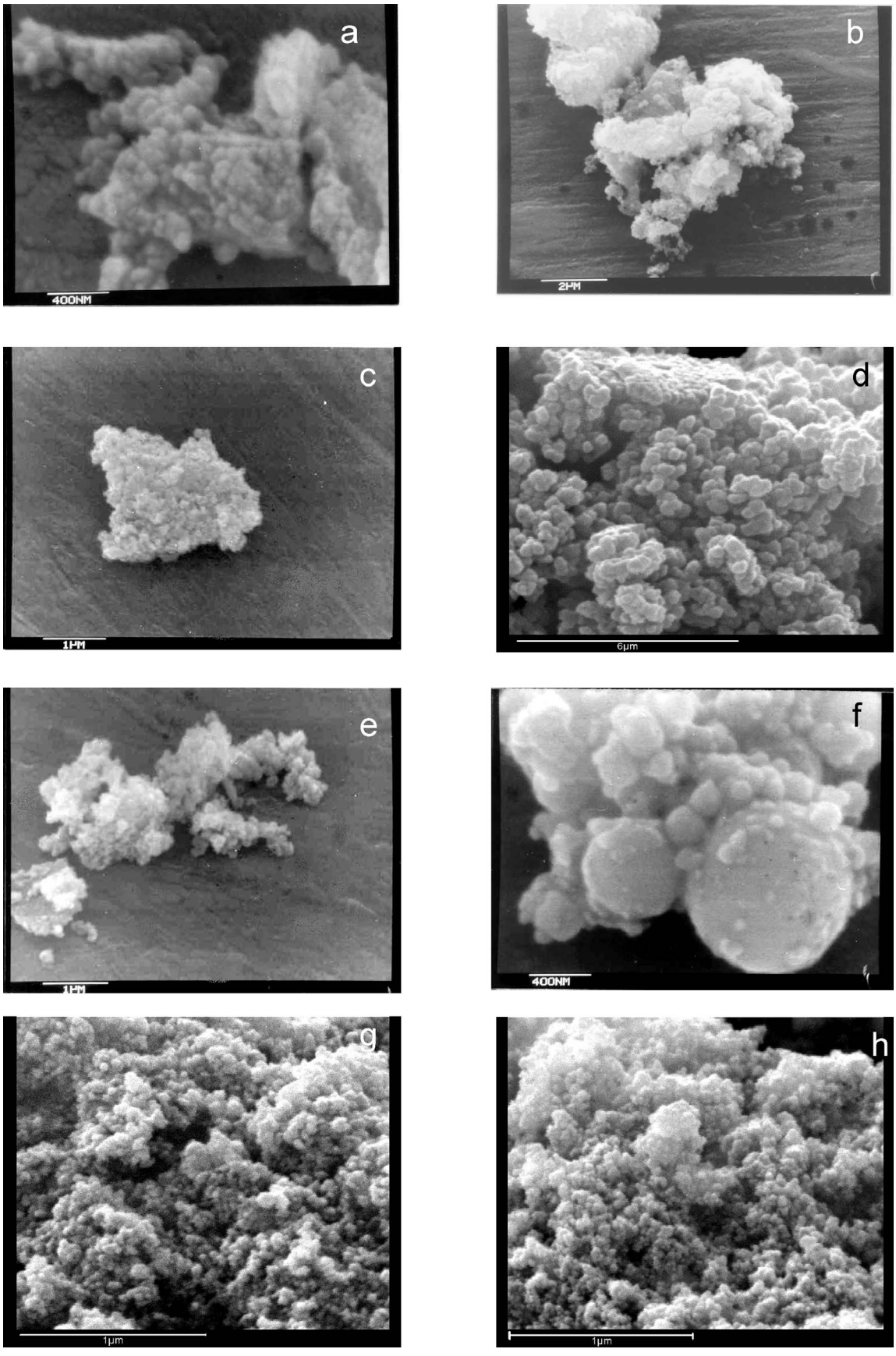

Fig. 3. Typical SEM micrographs of the various catalysts. (a) to (h): SGC-1, SGC-3, AgSGC-1, AgSGC-2.5, AgSGC-5, AgFH, FP, AgFP, in the order.

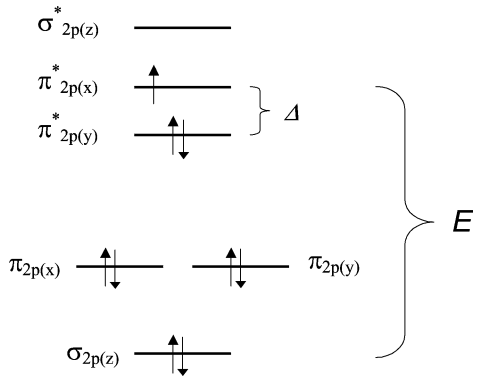

Fig. 4. Simplified scheme of the energy levels for the O_2^- ion in the presence of a crystal field.

Further information about the nature of the species catalytically active for the CFC of methane and about the valence of Ag ions and/or the possible presence of metallic Ag in our Ag-doped samples was collected by EPR analysis. For the $SrTiO_{3\pm\delta}$ samples, in a previous paper [22] it was shown that the presence of species more or less active for the present reaction depends on the catalyst preparation procedure. Indeed, in a catalyst prepared by the FH technique both the O_3^-/Ti^{4+} and O^-/Ti^{4+} couples were found in relatively high amounts, whereas in a sample prepared by the same technique, but with a different complexing agent (tartaric instead of citric acid), a greater amount of several O^-/Ti^{4+} species was found, accompanied by an increase in catalytic activity. In addition, the FH technique only led to a substantial formation of these species; the SGC technique led to samples in which titanium was present prevalently as Ti^{3+} ion.

Many papers in the literature deal with O_2^- ions adsorbed to oxide surfaces or interacting with cations in many systems [26]. In particular, Känzig and Cohen [27] derived a set of three equations for the g values of O_2^- ions involved in purely ionic interactions. These equations are based on the absolute value (152 cm^{-1}) of the oxygen spin-orbit interaction constant λ and on the Δ and E splittings of the energy levels for the same O_2^- species in the presence of a crystal field (Fig. 4). The lowest value of g_{xx}, calculated with these equations, is almost always very close to the value g_e of the free electron [28–33], and we confirmed this for the O_2^-/Ti^{4+} species in $SrTiO_{3\pm\delta}$ [22].

For the present AgFH sample, the EPR spectrum could be fitted, through the Bruker SimFonia programme (Fig. 5), with $g_{xx} = 2.007$, a value rather too high with respect to that (2.0021) calculated with the mentioned equations. However, a shift of the same order of magnitude for the g_{xx} value has frequently been reported and attributed either to coupling of O_2^- with the f-electrons of the metal cation [34–38] or to the presence of not completely ionic bonds [39,40], for which those equations can no longer be considered completely valid. Therefore, since virtually no trace of the Ag^{2+} pattern (vide infra) was noticed in the EPR spectrum of the present AgFH sample (Fig. 5), and the presence of metallic

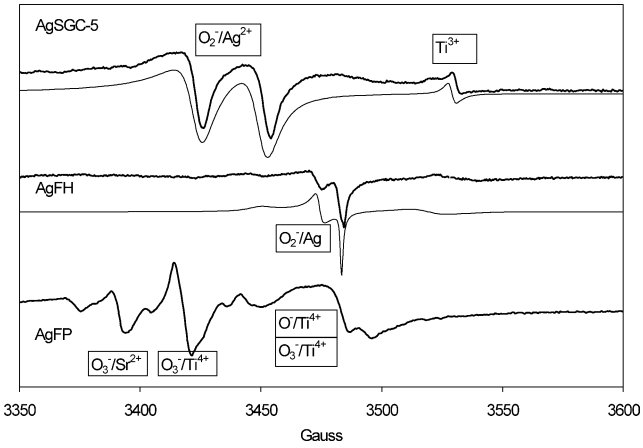

Fig. 5. Comparison of EPR spectra (at 290 K) of AgSGC-5, AgFH and AgFP samples. Thinner tracks: patterns simulated by means of the equations suggested in [27].

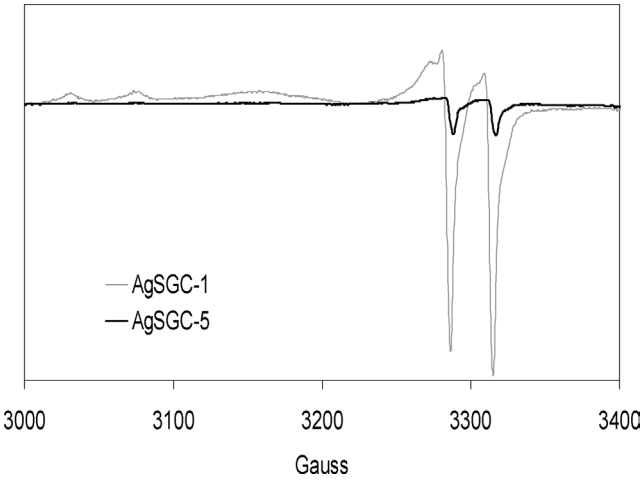

Fig. 6. EPR spectra of AgSGC-1 and AgSGC-5 catalysts.

Ag was shown by XRD analysis (Fig. 1), we can conclude that O_x^-/Ag couples would be present in this catalyst, similar to what was reported for O_2^- adsorbed to metallic Ag in other systems [40,41].

Furthermore, in Fig. 5 some lines can be observed in the EPR spectrum of AgFP that coincide perfectly with those found with the FP sample (here not shown) and with those found in a $SrTiO_{3\pm\delta}$ sample ([22], there labelled with T1), prepared by the FH procedure. Those lines were attributed to O_3^-/Ti^{4+}, to O^-/Sr^{2+}, and to different O^-/Ti^{4+} species leading to a higher activity of that catalyst [22].

In addition, the EPR spectra of the AgSGC-1 and AgSGC-5 catalysts are compared in Fig. 6. They are identical, except for intensity, which is 6 times lower for the latter catalyst, with respect to the former. These spectra can be unambiguously attributed to $4d^9$ Ag^{2+} ions, though the EPR evidence does not exclude the simultaneous presence of Ag^+ ions.

Indeed, no paramagnetic species other than Ag^{2+} can be hypothesised [42] to account for this EPR pattern. Though

relatively few papers only have been published up to date on Ag^{2+} species, because of the difficult stabilisation of such an oxidation state, an EPR spectrum practically identical to those of Fig. 6 has been observed since 1961 with Ag^{2+} in frozen solutions of HNO_3 or H_2SO_4 [43]. Ag^{2+} EPR spectra of this kind have also been reported for $Ag(SO_3F)_2$ [44,45], with $AgMF_6$ (M = Sn, Pb, Hf, Zr) and with $MAgF_4$ (M = Ba, Ca, Hg, Sr), in which Ag^{2+} centres were in either axially elongated tetragonal or in square-planar arrangements [46,47]. At last, spectra like these have been reported with many solid-state systems after γ-irradiation and attributed to Ag^{2+}. Among them, single crystals of $Ca(OD)_2$:Ag [48] and of $CdCl_2$:Ag [49], as well as AgX zeolites [50], may be cited. In the present case, the $4d^9$ Ag^{2+} electron resides in the d_{x2-y2} orbital embedded in a tetragonally elongated octahedral crystal, as indicated by the fact that $g_{\parallel} > g_{\perp}$ [42,51].

We suggest that Ag^{2+} is substituted for Sr^{2+} in the perovskitic structure, though the only compound known to date in the Ag–Ti–O ternary system is Ag_2TiO_3 [52]. Indeed, if Ag^{2+} were present as an extraframework AgO impurity, it would not contribute to the EPR pattern, because the latter contains alternating Ag^{+} and Ag^{3+} ions, leading to a diamagnetic system [53]. In any case, the presence of any other extraframework Ag^{2+}-containing impurities contributing to the EPR pattern seems very unlikely, because the EPR spectrum did not change after the sample was leached with nitric acid (vide infra). Furthermore, our XRD pattern (Fig. 1) excludes the possibility of the presence of any other Ag-containing phase, apart from traces of metallic Ag. Moreover, the substitution of Ag^{2+} for Sr^{2+} is in agreement with the above-mentioned decrease in cell volume indicated by Fig. 2. Such Ag^{2+} ions could interact with some O_x^- species, leading to O_x^-/Ag^{2+} couples. The nature of these O_x^- species is now under investigation. In addition, we cannot completely exclude the possibility of the presence of intra-crystalline Ag^{+} species, which are EPR silent. However, this oxidation state for Ag would be accompanied by a corresponding increase in lattice oxygen vacancies, a further oxidation of Ti beyond Ti^{4+} being extremely unlikely. In our opinion, however, these Ag^{+}-based species should be poorly active catalytically. Indeed, a similar parallel investigation on K-doped $SrTiO_3$ samples led in any case to scarcely active catalysts.

Finally, the presence of Ag^{2+} ions can hardly be observed in AgFP and is virtually excluded in AgFH EPR patterns (Fig. 5), which is further in line with the results of the XRD analysis (Fig. 2), which suggest a much more pronounced partial substitution of Ag^{2+} for Sr^{2+} in the AgSGC samples.

3.2. Catalytic activity

The results of catalytic activity comparison tests for the present catalysts are shown in Fig. 7. No relation was observed between catalytic activity and intensity of the Ti^{3+}

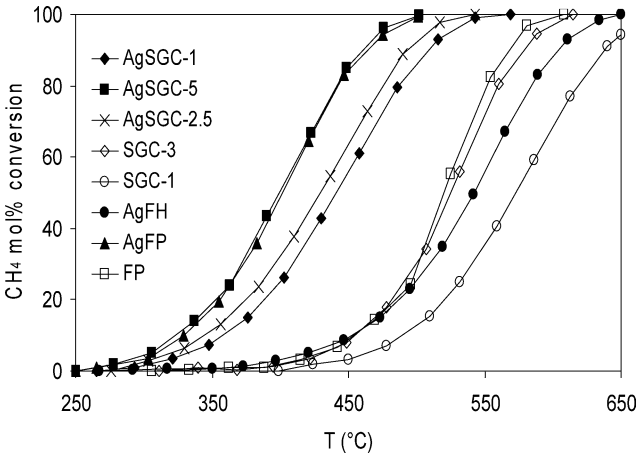

Fig. 7. Catalytic activity of the various catalysts.

EPR line (Fig. 5). Therefore, this species does not seem to be involved in the reaction. The superior performance of the Ag-doped versus undoped SGC catalysts is immediately evident. Indeed, the former lead to full conversion of CH_4 at $T_f < 570\,^{\circ}C$, whereas for the latter a T_f higher than 610 °C is needed to attain the same result. In principle the higher catalytic activity of the Ag-doped samples could be due to the presence of either metallic Ag, as suggested in some previous papers [54,55], or of Ag^{2+}-containing species, or of neither of them. Instead, it can be due to the presence of a higher concentration of oxygen-based species. With the aim of verifying the first of these hypotheses, the AgSGC-2.5 sample was repeatedly treated with a 4 wt% nitric acid solution, to oxidise and leach away most of the metallic Ag. The XRD analysis of the solid, recovered after the so-treated catalyst (referred to as AgSGC-2.5R), rinsed and dried overnight at 100 °C, showed a neat decrease in the weak pattern due to metallic Ag. This was accompanied by the appearance of Ag^{+} ions in the nitric leaching solution, confirmed through the usual precipitation of the corresponding amount of AgI after the addition of a KI solution. Furthermore, the EPR spectra of AgSGC-2.5 and AgSGC-2.5R showed an almost identical concentration of Ag^{2+} (Fig. 8), showing that Ag^{2+} species was practically unaffected by the nitric acid treatment. In addition, the conversion versus temperature curves of the activity tests carried out on the AgSGC-2.5 and AgSGC-2.5R samples overlapped perfectly (Fig. 9). Therefore, the role of the metallic Ag in the catalytic activity can be ruled out. Then, the higher activity of the SGC-prepared Ag-doped catalysts, with respect to the undoped ones, could be connected with the presence of the Ag^{2+}-based species. However, AgSGC-5 was shown to be more active than AgSGC-1 (Fig. 7), though the Ag^{2+} EPR spectrum was less intense with the former than with the latter (Fig. 6). Therefore, the concentration of Ag^{2+} species also does not seem to be directly related to the catalytic activity of these samples. Furthermore, the different activities (T_f ranging from ca. 502 to ca. 569 °C; Fig. 7) of the three AgSGC samples should be connected with the different con-

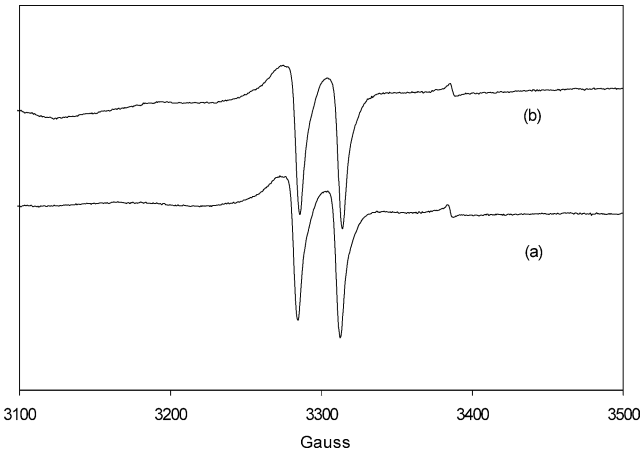

Fig. 8. EPR spectra of (a) AgSGC-2.5R and (b) AgSGC-2.5 samples.

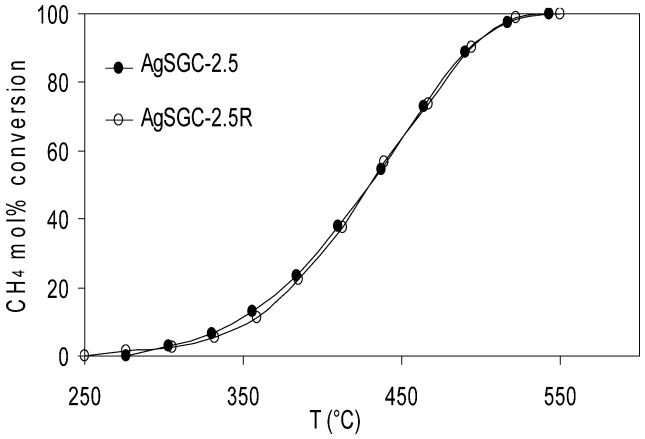

Fig. 9. Comparison of catalytic activity of AgSGC-2.5 and AgSGC-2.5R samples.

centrations of oxygen-based species, which in turn seem to be directly connected with the degree of disorder conferred by the different rates of temperature increase during preparation. In fact, the curves of AgSGC-2.5 and AgSGC-1 are progressively shifted, with T_f values of 550 and 570 °C, respectively.

A parallel behaviour can be noticed in a comparison of the activity of Ag-doped catalysts prepared by different methods (Fig. 7). The activity curves of AgFP and AgSGC-5 overlap almost perfectly, with T_f values of ca. 505 °C for both of them. This is in line with the observation that many oxygen-based species also appear in the EPR spectrum of AgFP, but different from AgFH (Fig. 5), which was shown to be the worst-performing catalyst of the set, with $T_f \cong 650$ °C. One may conclude that the O_x^-/Ag^{2+}-based species present in the AgSGC are characterised by catalytic activity comparable to that of the O_3^-/Ti^{4+}, O^-/Sr^{2+}, and O^-/Ti^{4+} species detected in AgFP by EPR analysis. In contrast, the O_x^-/Ag^{2+}-based species appear to be much more active than the O_x^-/Ag-based species present in AgFH (Fig. 5).

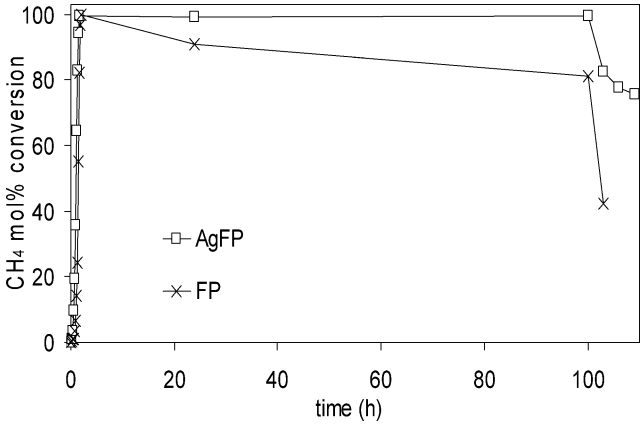

Fig. 10. Resistance to decaying of the catalysts prepared by the FP method.

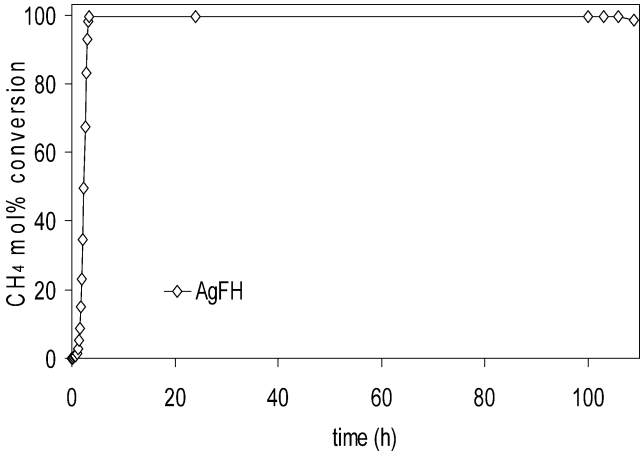

Fig. 11. Resistance to decaying of the catalysts prepared by the FH method.

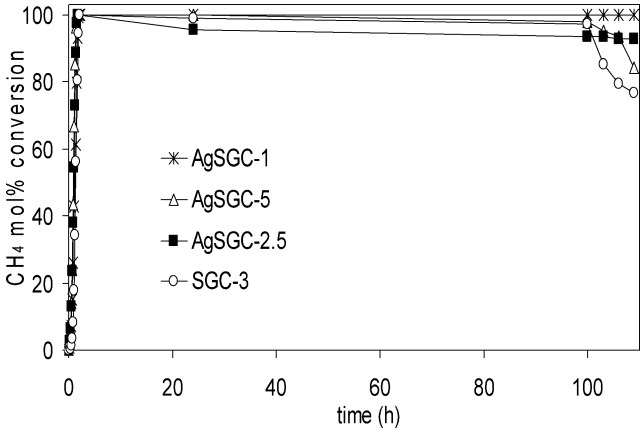

Fig. 12. Resistance to decaying of the catalysts prepared by the SGC method.

3.3. Thermal stability

A comparison of the thermal stability test data is reported in Figs. 10–12, for the catalysts prepared by the FP, FH, and SGC methods, respectively. It may be observed that in any case Ag doping significantly improves the stability of the catalyst; the CH_4 conversion after several accelerated

deactivation–reaction cycles is always much better for the Ag-doped samples. However, a noticeable difference in the resistance to high-temperature treatment is conferred by the three preparation procedures tested here.

The catalysts prepared by the FP method (Fig. 10) proved to be the less resistant. Indeed, the AgFP sample appeared rather stable after 100 h on stream, but, after the first deactivation–reaction cycle, CH_4 conversion dropped to 82%, and dropped further to 75% after the third cycle. The deactivation rate was much more pronounced for the FP sample, for which conversion hardly attained 80% after 100 h on stream and dropped to 42% after the first deactivation–reaction cycle only.

The catalysts prepared by the FH method proved the most resistant (Fig. 11). The FH sample showed a CH_4 conversion of 98% after 100 h on stream and of over 91% after the third deactivation–reaction cycle, whereas the AgFH was shown to attain a CH_4 conversion of 98.5% after the third deactivation–reaction cycle.

As for the catalysts prepared by the SGC method (Fig. 12), the best-performing sample was AgSGC-1, showing a CH_4 conversion of over 99% after the third deactivation–reaction cycle. A similar behaviour was shown by AgSGC-2.5. In spite of a small decrease in conversion (96.5%) after only 25 h on stream, its activity decayed very slowly, ensuring a 93% conversion after the third deactivation–reaction cycle. When the rate of temperature increase during preparation (AgSGC-5 sample) was increased, the activity increased (Fig. 7), but at the expense of a lower thermal stability (Fig. 12). Indeed, while remaining rather stable after 100 h on stream, partly due also to the relatively low value of T_f (502 °C), the conversion dropped to 83% after the third deactivation–reaction cycle. As indicated by EPR and XRD analysis (vide supra), the higher the rate of temperature increase during preparation, the lower was the concentration of intra-crystalline Ag^{2+} and the higher the amount of inter-particle metallic Ag in the catalyst. The latter confers a better resistance to sintering on the perovskite nanoparticles, by keeping them better separated from each other. Finally, in this case the worst catalyst was shown to be the undoped sample (SGC-3). Indeed, in spite of a rather slow deactivation rate, similar to that of AgSGC-5, during the first 100 h on stream, conversion dropped to 77% after the third deactivation–reaction cycle.

A further test was finally carried out with the AgSGC-2.5R catalyst, aimed at checking the effect of nitric acid treatment on thermal stability. Even though the activity was shown to be practically unaffected by such a treatment (Fig. 9), the thermal stability was rather poor (Fig. 13). In fact, the CH_4 conversion decreased considerably even after 24 h on stream and further dropped drastically after the first deactivation–reaction cycle only. This further confirms the protective action of inter-particle Ag against perovskite sintering.

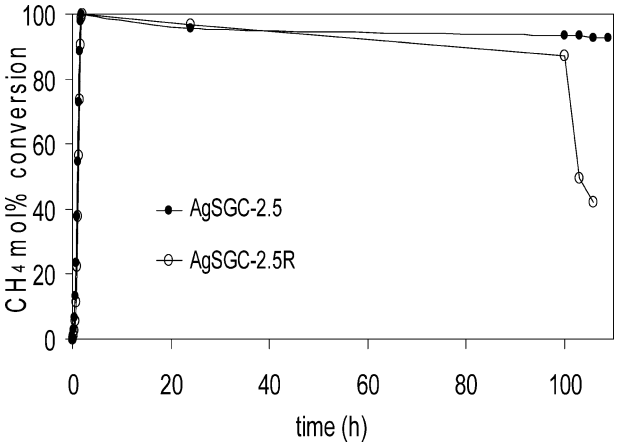

Fig. 13. Comparison of resistance to decaying of the AgSGC-2.5 and AgSGC-2.5R catalysts.

4. Conclusions

Perovskite-structured $SrTiO_{3\pm\delta}$, especially $Sr_{0.9}Ag_{0.1}TiO_{3\pm\delta}$, was confirmed to be among the best substitutes for noble-metal-based catalysts for the CFC of methane under lean-burn conditions. For the same overall nominal composition, catalyst activity and durability depend strongly on the method of preparation. Indeed, for the samples prepared by the same method, a longer residence time at a given temperature during preparation entrains a higher durability, but a lower catalytic activity. In $Sr_{0.9}Ag_{0.1}TiO_{3\pm\delta}$ catalysts Ag is present either as intra-crystalline Ag^{2+}, likely substituting for Sr^{2+} in the perovskite lattice, or as inter-crystalline metallic Ag. However, the catalytic activity of these samples is not directly related to these Ag species, but to the presence of O^-/Ti^{4+}, O_2^-/Ti^{4+}, O_3^-/Ti^{4+}, O^-/Sr^{2+}, and O_x^-/Ag^{2+} or O_x^-/Ag, the last being less active than the others. Furthermore, inter-crystalline metallic Ag plays an important role in improving catalyst resistance to sintering, the most durable catalysts being those calcined for a sufficient residence time at the highest temperature during preparation, that is, under conditions better favouring the segregation of this metal from the perovskite lattice.

Acknowledgment

The valuable help of Dr. M. Scavini in the interpretation of XRD patterns is gratefully acknowledged.

References

[1] M.F. Zwinkels, S.G. Järås, P.G. Menon, Catal. Rev. Sci. Eng. 25 (1993) 319.
[2] H. Arai, M. Machida, Catal. Today 10 (1991) 81.
[3] K. Eguchi, H. Arai, Catal. Today 29 (1996) 379.
[4] H. Davy, in: J. Davy (Ed.), The Collected Works of Sir Humphrey Davy, vol. 6, Smith, Elder and Co., Cornhill, London, 1840.

[5] J. Arbiol, A. Cabot, J.R. Morante, F. Chen, M. Liu, Appl. Phys. Lett. 81 (2002) 3449.
[6] J.L.G. Fierro, in: L.G. Tejuca, J.L.G. Fierro (Eds.), Properties and Applications of Perovskite-Type Oxides, Dekker, New York, 1993.
[7] M.A. Peña, J.L.G. Fierro, Chem. Rev. 101 (2001) 1981.
[8] L. Marchetti, L. Forni, Appl. Catal. B: Environ. 15 (1998) 179.
[9] D. Ferri, L. Forni, Appl. Catal. B: Environ. 16 (1998) 119.
[10] C. Oliva, L. Forni, Appl. Magn. Res. 18 (2000) 475.
[11] R.A.M. Giacomuzzi, M. Portinari, I. Rossetti, L. Forni, in: A. Corma, F.V. Melo, S. Mendioroz, J.L.G. Fierro (Eds.), in: Stud. Surf. Sci. Catal., vol. 130, Elsevier, Amsterdam, 2000, p. 197.
[12] R. Leanza, I. Rossetti, L. Fabbrini, C. Oliva, L. Forni, Appl. Catal. B: Environ. 28 (2000) 55.
[13] C. Oliva, L. Forni, A. D'Ambrosio, F. Navarrini, A.D. Stepanov, Z.D. Kagramanov, A.I. Mikhailichenko, Appl. Catal. A: Gen. 205 (2001) 245.
[14] I. Rossetti, L. Forni, Appl. Catal. B: Environ. 33 (2001) 345.
[15] L. Forni, I. Rossetti, Appl. Catal. B: Environ. 38 (2002) 29.
[16] L. Fabbrini, I. Rossetti, L. Forni, Appl. Catal. B: Environ. 44 (2003) 107.
[17] L. Fabbrini, I. Rossetti, L. Forni, Appl. Catal. B: Environ. 56 (2005) 221.
[18] M.G.S. Baythoun, F.R. Sale, J. Mater. Sci. 17 (1982) 2757.
[19] H.M. Zhang, Y. Teraoka, N. Yamazoe, Chem. Lett. 1 (1987) 665.
[20] L. Mädler, H. Kammler, R. Mueller, S. Pratsinis, Aerosol Sci. 33 (2002) 369.
[21] R. Strobel, L. Mädler, W.J. Stark, S.E. Pratsinis, A. Baiker, J. Catal. 213 (2003) 296.
[22] C. Oliva, L. Bonoldi, S. Cappelli, L. Fabbrini, I. Rossetti, L. Forni, J. Mol. Catal. A: Chem. 226 (2005) 33.
[23] R.N. Das, P. Pramanik, Brit. Ceram. Trans. 99 (2000) 153.
[24] Selected Powder Diffraction Data, JCPDS, Swarthmore, PA, file 5-418.
[25] Selected Powder Diffraction Data, JCPDS, Swarthmore, PA, file 01-1167.
[26] M. Che, A.J. Tench, in: D.D. Eley, H. Pines, P.B. Weisz (Eds.), Advances in Catalysis, vol. 32, Academic Press, San Diego, 1983, p. 1.
[27] W. Känzig, M.H. Cohen, Phys. Rev. Lett. 3 (1959) 509.
[28] A. Tuel, J. Diab, P. Gelin, M. Dufaux, J.-F. Dutel, Y. Ben Taarit, J. Mol. Catal. 63 (1990) 95.
[29] C. Louis, T. Lin Chang, M. Kermarec, T. Le Van, J.M. Tatibouet, M. Che, Colloids Surf. A: Physicochem. Engin. Aspects 72 (1993) 217.
[30] T. Yang, L. Feng, S. Shen, J. Catal. 145 (1994) 384.
[31] K. Dyrek, A. Adamski, Z. Sojka, Spectrochim. Acta, Part A 54 (1998) 2337.
[32] A.L. Attwood, D.M. Murphy, J.L. Edwards, T.A. Egerton, R.W. Harrison, Res. Chem. Intermed. 29 (2003) 449.
[33] A.L. Attwood, J.L. Edwards, Ch.C. Rowlands, D.M. Murphy, J. Phys. Chem. 107 (2003) 1779.
[34] M. Setaka, T. Kwan, Bull. Chem. Soc. Jpn. 43 (1970) 2727.
[35] M. Gideon, M. Steiberg, J. Solid State Chem. 4 (1972) 370.
[36] M. Che, J.F.J. Kibblewhite, A.J. Tench, M. Dufaux, C. Naccache, J. Chem. Soc. Faraday Trans. I 69 (1973) 857.
[37] A.S. Sass, V.A. Shvets, G.A. Savel'eva, N.M. Popova, V.B. Kazanskii, Kinet. Katal. 26 (1985) 924.
[38] J. Soria, J.M. Coronado, J.C. Conesa, J. Chem. Soc. Faraday Trans. I 92 (1996) 1619.
[39] Ch.-A. Jenkins, D.M. Murphy, J. Phys. Chem. B 103 (1999) 1019.
[40] G. Li, X. Wang, X. Guo, S. Liu, Q. Zhao, Z. Bao, L. Lin, Mater. Chem. Phys. 71 (2001) 195.
[41] R.B. Clarkson, S. McClellan, J. Phys. Chem. 82 (1978) 325.
[42] J.E. Wertz, J.R. Bolton, Electron Spin Resonance, McGraw-Hill, New York, 1972, p. 289.
[43] J.A. McMillan, B. Smaller, J. Chem. Phys. 35 (1961) 1698.
[44] P.C. Leung, F. Aubke, Inorg. Chem. 17 (1978) 1765.
[45] P.C. Leung, K.C. Lee, F. Aubke, Can. J. Chem. 57 (1979) 326.
[46] G.C. Allen, R.F. McMeeking, J. Chem. Soc. Dalton (1976) 1063.
[47] G.C. Allen, R.F. McMeeking, R. Hoppe, B. Muller, J. Chem. Soc. Chem. Commun. (1972) 291.
[48] F. Holuj, J. Magn. Reson. 51 (1983) 37.
[49] T. Miyanaga, K. Kan'no, S. Naoé, H. Matsumoto, J. Phys. Soc. Jpn. 30 (1971) 1669.
[50] N. Kanzaki, I. Yasumori, J. Phys. Chem. 82 (1978) 2351.
[51] N.M. Atherton, Electron Spin Resonance, Wiley, London, 1973, p. 197.
[52] C. Linke, M. Jansen, J. Solid State Chem. 134 (1997) 17.
[53] J.A. McMillan, Chem. Rev. 62 (1962) 65.
[54] W. Wang, H. Zhang, G. Lin, Z. Xiong, Appl. Catal. B: Environ. 24 (2000) 219.
[55] B. Kucharczyk, W. Tylus, Catal. Today 90 (2004) 121.